APPENDIX A

SAR System Validation for the 802.11 b/g Bands

The measured SAR distribution for the peak 1-g SAR region using a reference dipole at 2450 MHz.

For July 1, 2003

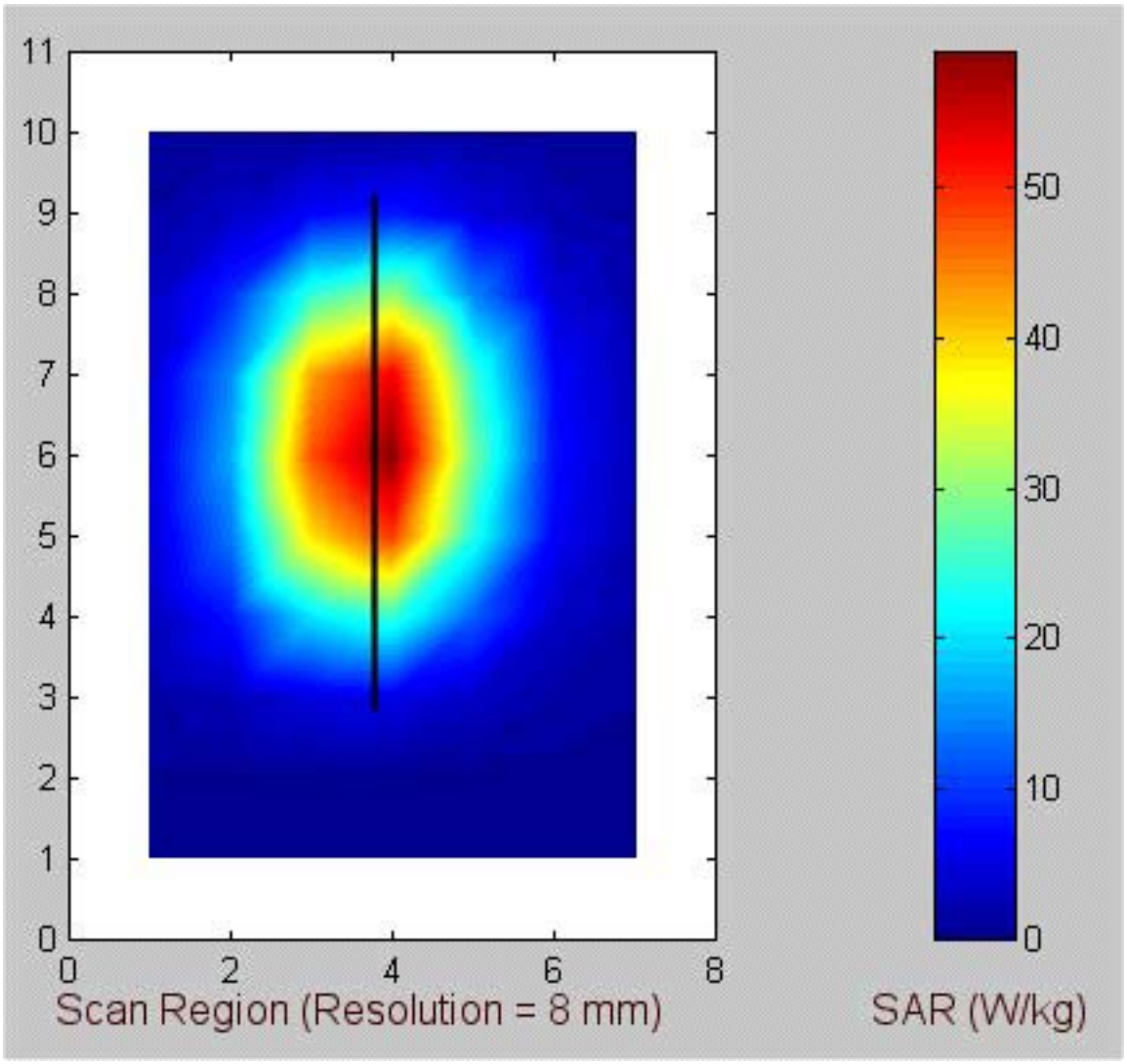

Fig. A.1. Coarse scans of the measured SAR distribution for the reference dipole used for system validation at 2.45 GHz. Also shown is the outline of the reference dipole overlaid on the SAR contours. Radiated power = 1 W.

1-g SAR = 52.150 W/kg

a. At depth of 1 mm

72.414	81.546	85.194	82.881	75.448
74.762	83.950	87.658	85.543	77.915
76.010	85.205	88.968	86.788	79.073
76.064	85.476	88.690	86.349	78.557
74.869	83.481	86.911	84.453	76.160

b. At depth of 3 mm

57.420	64.040	66.586	64.851	59.361
59.251	65.979	68.596	67.045	61.302
60.270	66.938	69.600	67.921	62.183
60.241	67.139	69.492	67.725	61.929
59.294	65.684	68.113	66.335	60.080

c. At depth of 5 mm

44.655	49.212	50.858	49.601	45.720
46.050	50.747	52.478	51.386	47.224
46.876	51.474	53.236	51.980	47.872
46.792	51.615	53.252	51.961	47.822
46.055	50.589	52.209	50.980	46.428

d. At depth of 7 mm

34.119	37.061	38.009	37.134	34.526
35.156	38.254	39.304	38.566	35.682
35.827	38.811	39.875	38.964	36.141
35.718	38.902	39.970	39.056	36.235
35.151	38.197	39.199	38.387	35.203

e. At depth of 9 mm

25.813	27.587	28.040	27.448	25.778
26.572	28.501	29.075	28.585	26.674
27.124	28.951	29.519	28.872	26.988
27.017	29.001	29.645	29.011	27.168
26.582	28.508	29.082	28.557	26.407

APPENDIX B

SAR System Validation for the 802.11a Band

The measured SAR distribution for the peak 1-g SAR region using WR 187 rectangular waveguide irradiation system.

For July 1, 2003 – The SAR plot at 5.25 GHz

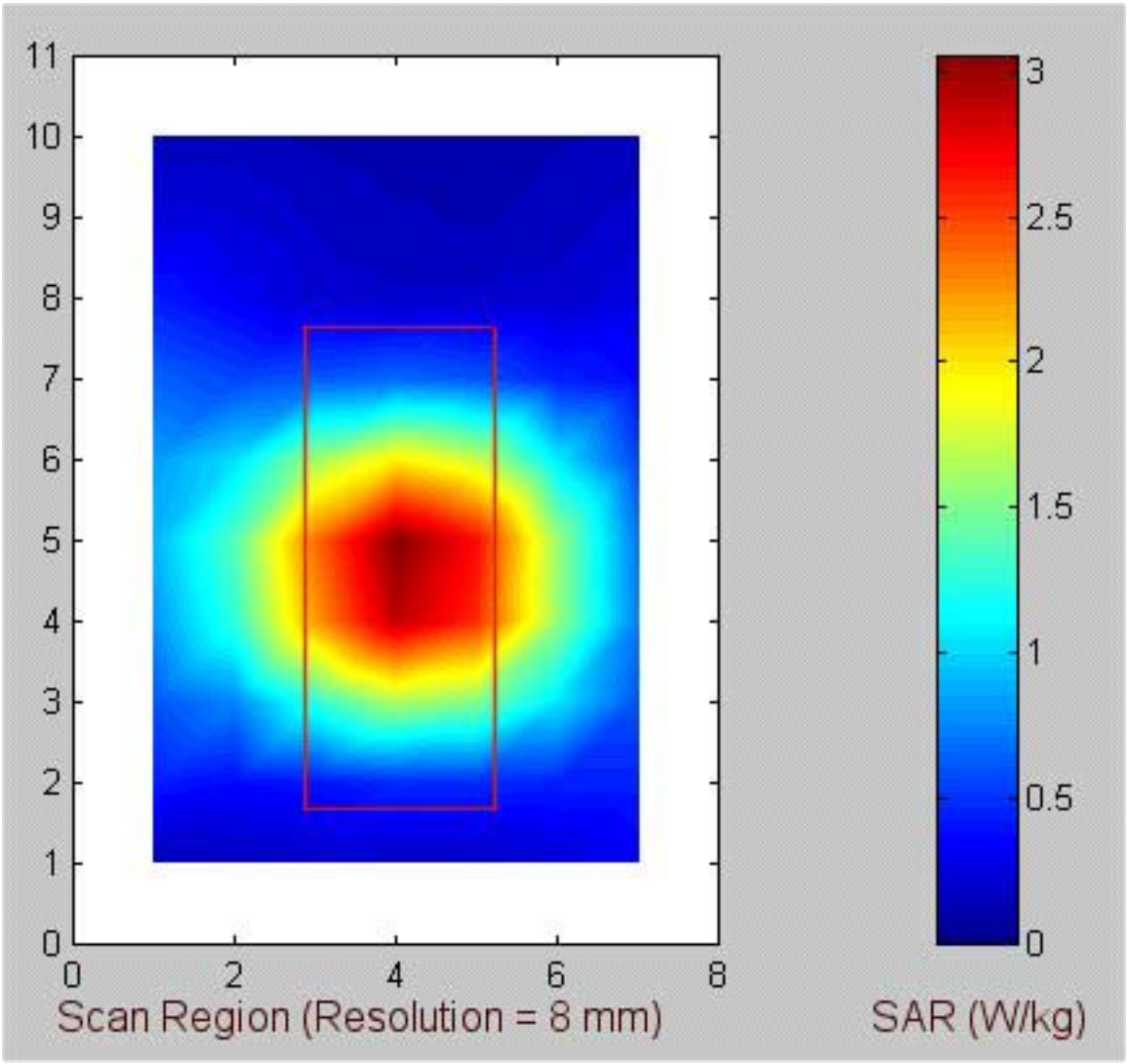

Fig. B.1. Coarse scans of the measured SAR distribution for the WR187 rectangular waveguide irradiation system for system verification at 5.25 GHz. Also shown is the outline of the rectangular waveguide overlaid on the SAR contours. Radiated power = 100 mW.

1-g SAR = 3.612 W/kg

a. At depth of 1 mm

8.978	9.511	9.821	9.760	9.378
9.630	9.920	10.313	10.263	9.827
9.940	10.492	10.467	10.510	10.138
9.776	10.178	10.439	10.536	10.118
9.637	9.883	10.119	10.116	9.808

b. At depth of 3 mm

4.110	4.327	4.445	4.448	4.328
4.386	4.560	4.700	4.684	4.541
4.525	4.761	4.792	4.806	4.675
4.484	4.658	4.786	4.807	4.646
4.393	4.541	4.640	4.642	4.507

c. At depth of 5 mm

1.793	1.870	1.907	1.935	1.895
1.894	1.985	2.037	2.028	1.995
1.947	2.048	2.080	2.088	2.044
1.945	2.019	2.083	2.076	2.023
1.898	1.973	2.026	2.032	1.971

d. At depth of 7 mm

0.870	0.900	0.909	0.939	0.907
0.905	0.947	0.976	0.970	0.958
0.922	0.979	0.994	0.999	0.977
0.924	0.962	0.995	0.984	0.965
0.910	0.940	0.979	0.985	0.955

e. At depth of 9 mm

0.537	0.556	0.553	0.577	0.544
0.550	0.574	0.586	0.591	0.572
0.558	0.601	0.601	0.599	0.585
0.558	0.583	0.597	0.590	0.580
0.561	0.574	0.599	0.600	0.589

For July 1, 2003 – The SAR plot at 5.8 GHz

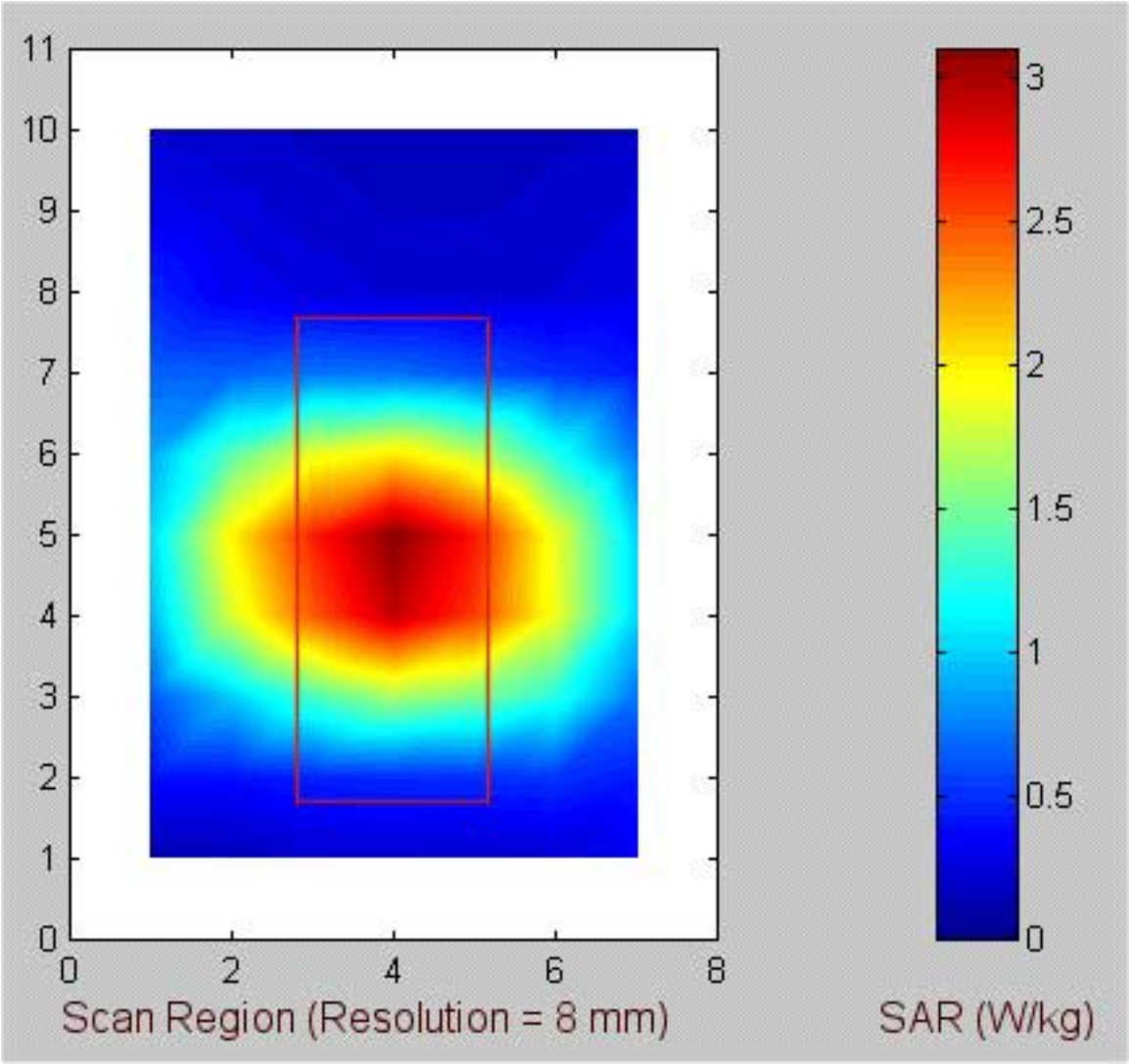

Fig. B.2. Coarse scans of the measured SAR distribution for the WR187 rectangular waveguide irradiation system for system verification at 5.8 GHz. Also shown is the outline of the rectangular waveguide overlaid on the SAR contours. Radiated power = 100 mW.

1-g SAR = 3.825 W/kg

a. At depth of 1 mm

10.317	10.828	10.724	10.702	10.216
11.002	11.307	11.416	11.320	10.588
11.240	11.569	11.570	11.497	10.742
11.313	11.592	11.419	11.332	10.948
10.915	11.068	11.285	10.970	10.621

b. At depth of 3 mm

4.520	4.681	4.671	4.647	4.493
4.765	4.915	4.969	4.875	4.635
4.859	5.015	5.045	4.966	4.740
4.882	5.006	5.006	4.918	4.750
4.714	4.808	4.869	4.763	4.597

c. At depth of 5 mm

1.831	1.852	1.870	1.855	1.817
1.890	1.951	1.984	1.918	1.871
1.918	1.980	2.003	1.963	1.916
1.926	1.976	2.005	1.946	1.887
1.860	1.916	1.924	1.897	1.829

d. At depth of 7 mm

0.827	0.815	0.831	0.821	0.804
0.829	0.851	0.869	0.835	0.833
0.835	0.854	0.860	0.855	0.838
0.845	0.858	0.868	0.841	0.826
0.810	0.842	0.842	0.837	0.812

e. At depth of 9 mm

0.519	0.510	0.519	0.508	0.488
0.509	0.524	0.522	0.511	0.508
0.513	0.519	0.514	0.514	0.503
0.530	0.514	0.516	0.506	0.507
0.498	0.514	0.515	0.518	0.507

APPENDIX C

AN OPEN-ENDED WAVEGUIDE SYSTEM FOR SAR SYSTEM VALIDATION AND/OR PROBE CALIBRATION FOR FREQUENCIES ABOVE 3 GHz

Qingxiang Li, Student Member, IEEE
Om P. Gandhi, Life Fellow, IEEE, and
Gang Kang, Senior Member, IEEE
Department of Electrical and Computer Engineering
University of Utah
Salt Lake City, Utah 84112, U.S.A.

Abstract

Compliance with safety guidelines prescribed in terms of maximum electromagnetic power absorption (specific absorption rate or SAR) for any 1- or 10-g of tissue is required for all newly-introduced personal wireless devices such as Wi-Fi PCs. The prescribed SAR measuring system is a planar phantom with a relatively thin base of thickness 2.0 mm filled with a lossy fluid to simulate dielectric properties of the tissues. A well-characterized, broadband irradiator is required for SAR system validation and/or submerged E-field probe calibration for the new 802.11a frequencies in the 5-6 GHz band. We describe an open-ended waveguide system that may be used for this purpose. Using a fourth-order polynomial least-square fit to the experimental data gives SAR variations close to the bottom surface of the phantom that are in excellent agreement with those obtained using the FDTD numerical method. The experimentally-determined peak 1-g SARs are within 1 to 2 percent of those obtained using the FDTD both at 5.25 and 5.8 GHz.

Index Terms – Broadband, electromagnetic exposure system, probe calibration, safety assessment, comparison with numerical calculations

Submitted to *IEEE Transactions on Microwave Theory and Techniques*, June 10, 2003.

AN OPEN-ENDED WAVEGUIDE SYSTEM FOR SAR SYSTEM VALIDATION AND/OR PROBE CALIBRATION FOR FREQUENCIES ABOVE 3 GHz

Qingxiang Li, Student Member, IEEE
Om P. Gandhi, Life Fellow, IEEE, and
Gang Kang, Senior Member, IEEE

I. Introduction

Compliance with the safety guidelines such as those proposed by IEEE [1] ICNIRP [2], etc. is required by regulatory agencies in the United States and elsewhere for all newly-introduced personal wireless devices such as Wi-Fi PCs, cellular telephones, etc. These safety guidelines are set in terms of maximum 1- or 10-g mass-normalized rates of electromagnetic energy deposition (specific absorption rates or SARs) for any 1- or 10-g of tissue. The two most commonly-used SAR limits today are those of IEEE [1] – 1.6 W/kg for any 1 g of tissue, and ICNIRP [2] – 2 W/kg for any 10 g of tissue, excluding extremities such as hands, wrists, feet, and ankles where higher SARs up to 4 W/kg for any 10 g of tissue are permitted in both of these standards. Experimental and numerical techniques using planar or head-shaped phantoms have been proposed for determining compliance with the SAR limits [3-5]. For frequencies above 800 MHz, the size of a rectangular waveguide is quite manageable and use of an appropriate waveguide filled with a tissue-simulant medium is recommended for calibration of an E-field probe in FCC Supplement C, Edition 01-01 to OET Bulletin 65 [6]. Even though no recommendation is made on choice of an irradiation system for frequencies above 3 GHz, balanced half-wave dipoles have been suggested for system validation for frequencies less than or equal to 3 GHz [6]. It is very difficult to develop half-wave dipole antennas for use in the 5.1 to 5.8 GHz band both because of fairly small dimensions and the resulting dimensional tolerances, and relatively narrow bandwidths of the required baluns – balanced to unbalanced transformers (typically less than 10-12% for VSWR < 2.0 and less than 5-6% for VSWR < 1.5). On the other hand, rectangular waveguides are broadband with simultaneous bandwidths larger than 1-2 GHz and are fairly easy to use for frequencies in excess of 3 GHz. We have, therefore, developed an open-ended waveguide system for SAR system validation and/or probe calibration in the frequency band 5 to 6 GHz. This is a band that is presently being used for 802.11a antennas of Wi-Fi PCs.

II. The Waveguide Irradiation System

For the 5-6 GHz band, we have used a WR187 rectangular waveguide of internal dimensions 4.75 × 2.21 cm. The operating (TE_{10} mode) band of this waveguide is from 3.95 to 5.85 GHz. This is considerably larger than the required overall bandwidth of 675 MHz for the IEEE 802.11a frequency bands of 5.15-5.35 and 5.745 to 5.825 GHz. The waveguide irradiation system used for SAR system validation is shown in Fig. 1. As recommended in [6], the open-ended waveguide irradiator is placed at a distance of 8 mm below the base of planar phantom with inside dimensions of 30.5 × 41.9 cm and a base thickness of 2.0 ± 0.2 mm. This results in the open end of the waveguide at a distance of 10 mm below the lossy tissue-simulant fluid in the phantom. The microwave circuit arrangement used for the waveguide irradiation system is shown in Fig. 2. As shown in Fig. 2, the WR187 waveguide is fed with microwave power from a

Hewlett Packard Model 83620A Synthesized Sweeper (10 MHz-20 GHz). When placed at a distance of 8 mm below the base of the planar phantom, the reflection coefficient is about 10-20%. Even this relatively small amount of reflection has been greatly reduced to less than 0.5% by using a movable slide-screw waveguide tuner (Narda Model 22CI). The planar phantom is filled to a depth of 15 cm with a fluid to simulate dielectric properties recommended for the body phantom in [6]. The dielectric constants ε_r and conductivities σ at the experimental frequencies of 5.25 and 5.8 GHz are those recommended in the SAR Compliance Standards used in the U.S. and in Europe [3, 4]: $\varepsilon_r = 49.0$, $\sigma = 5.30$ S/m at 5.25 GHz; and $\varepsilon_r = 48.2$, $\sigma = 6.00$ S/m at 5.8 GHz.

Fig. 1. Photograph of the rectangular waveguide radiator used for system validation. Also seen is the Narda Model 22CI movable slide screw tuner used to match the input power at 5.25 or 5.8 GHz to the planar tissue-simulant phantom.

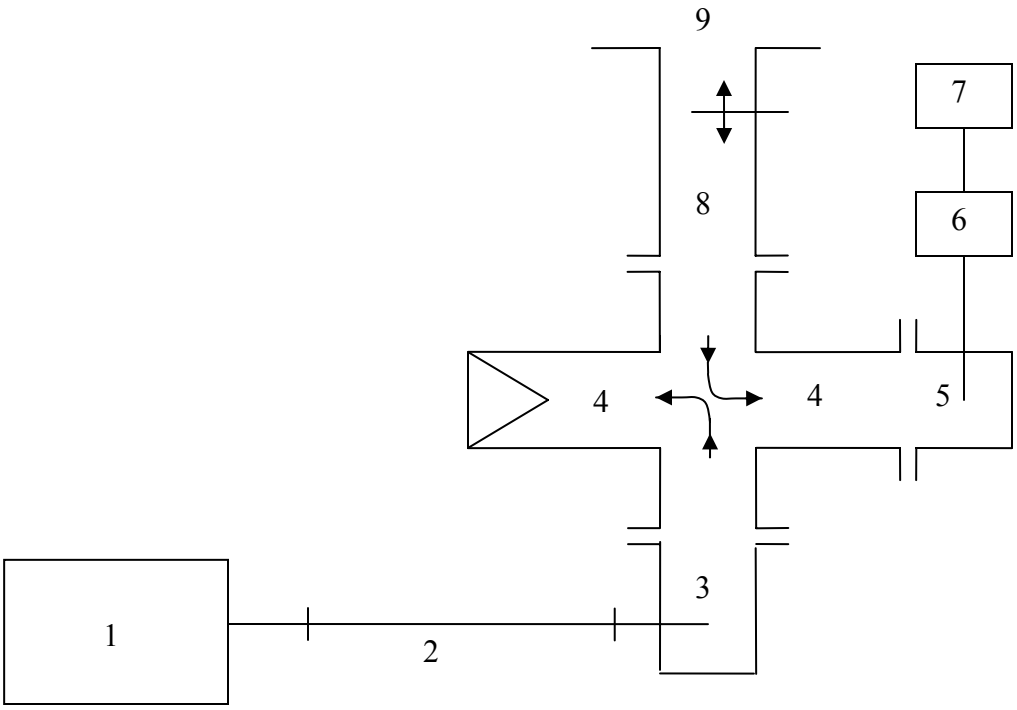

1. Hewlett Packard (HP) Model 83620A Synthesized Sweeper (10 MHz-20 GHz).
2. Coaxial line.
3. Coaxial to waveguide adapter.
4. 20 dB crossguide coupler (may be reversed to measure incident power).
5. HP Model G281A coaxial to waveguide adapter
6. HP Model 8482A power sensor.
7. HP Model 436A power meter.
8. Narda Microline® Slide Screw Tuner Model 22CI.
9. Radiating open end of the waveguide.

Fig. 2. The microwave circuit arrangement used for SAR system validation.

III. Calculation of the SAR Distributions

We have used the well-established finite-difference time-domain (FDTD) numerical electromagnetic method to calculate the electric fields and SAR distributions for the planar phantom of base thickness 2.0 mm of dielectric constant $\varepsilon_r = 2.56$ and dielectric properties of the tissue-simulant lossy fluid as given in Section II. The FDTD method described in several texts [7, 8] has been successfully used by various researchers [9-12] and, therefore, would not be described here. For the FDTD calculations, we have used a cell size $\delta = 0.5$ mm in order to meet the requirement $\delta \leq \lambda_\varepsilon / 10$ in the lossy fluid. The calculated variations of the SAR distribution at the experimental frequencies of 5.25 and 5.80 GHz are given in Figs. 3 a-c and 4

a-c, respectively. Also shown in the same figures are the experimental values of the SARs (shown by circles). From Figs. 3 and 4, it is obvious that the penetration of electromagnetic fields in the 5.1 to 5.8 GHz band is extremely shallow. The calculated depths of penetration corresponding to $1/e^2$-reduction of SAR (13.5% of the SAR at the surface) are only 6.85 and 5.985 mm at 5.25 and 5.8 GHz, respectively. Both of these depths of penetration are very similar to those obtained for plane-wave irradiation at these frequencies (7.15 mm for 5.25 GHz and 6.25 mm for 5.8 GHz).

IV. Experimental Setup and Measurements

A. *Experimental Setup*

As recommended in FCC Bulletin 65 [14], a planar phantom of fairly thin base thickness 2.0 mm of relatively low dielectric constant ($\varepsilon_r = 2.56$ in our case) is used for the determination of SAR distributions of wireless PCs and for the SAR system validation. The lateral dimensions of the planar phantom (in our case 30.5 × 41.9 cm) are large enough to ignore scattering from the edges of the rectangular box or the tissue-simulant lossy fluid used to fill this box to a depth of 10-15 cm (several times the depth of penetration of fields in the fluid so as to present a nearly infinitely deep medium to neglect reflections). A photograph of the phantom model together with a computer-controlled 3-D stepper motor system (Arrick Robotics MD-2A) is shown in Fig. 5.

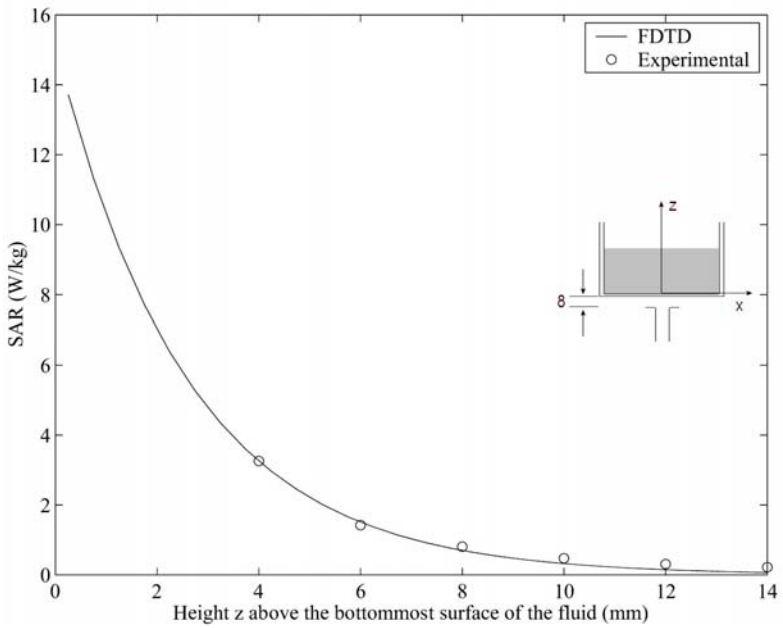

a. Variation of SAR along the z-axis.

Fig. 3. Comparison of the measured and calculated SAR variations for a planar phantom of base thickness 2.0 mm and internal dimensions 30.5 × 41.9 × 20 cm for a WR 187 open-ended waveguide radiator placed 10 mm below the bottommost surface of the lossy tissue-simulant phantom. Frequency = 5.25 GHz.

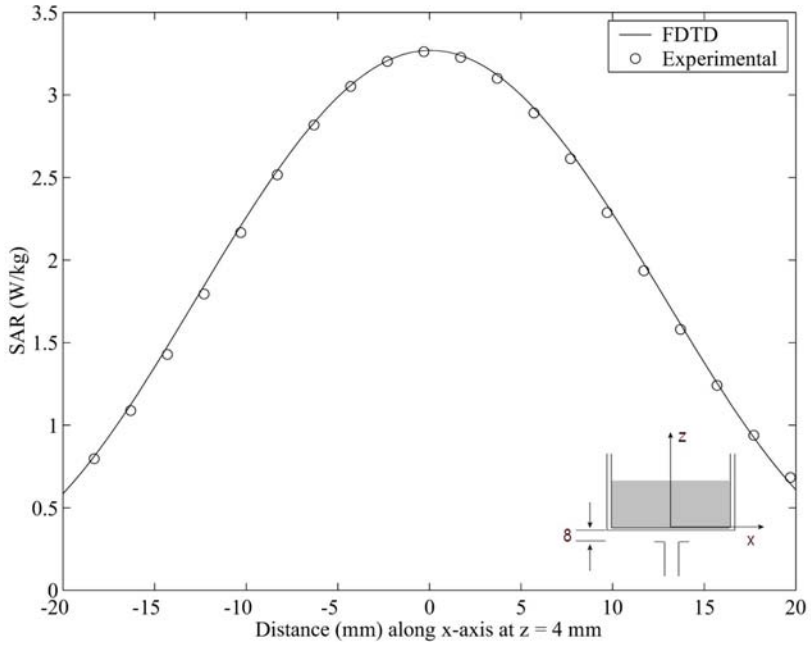

b. Variation of SAR along the x-axis parallel to the broader dimension of the waveguide at height z = 4 mm.

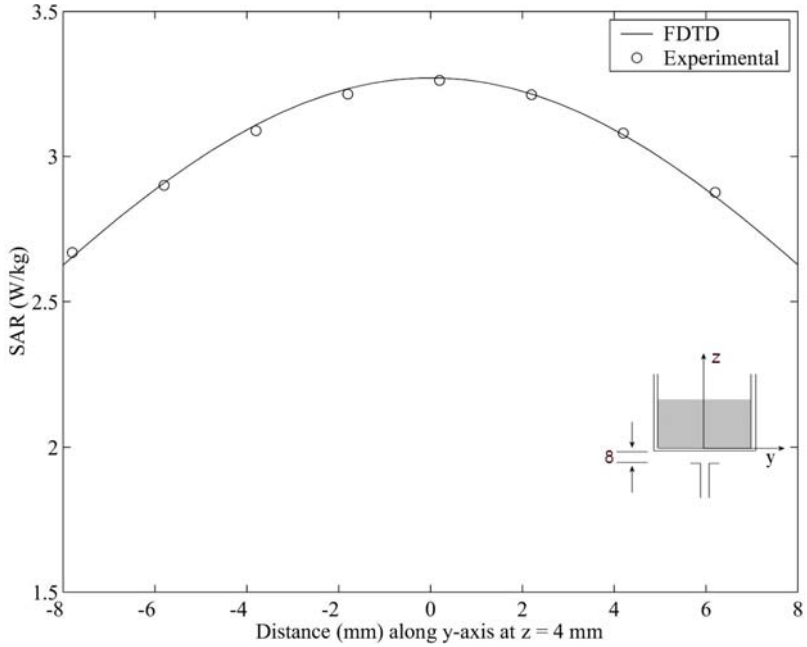

c. Variation of SAR along the y-axis parallel to the narrower dimension of the waveguide at height z = 4 mm.

Fig. 3. Comparison of the measured and calculated SAR variations for a planar phantom of base thickness 2.0 mm and internal dimensions 30.5 × 41.9 × 20 cm for a WR 187 open-ended waveguide radiator placed 10 mm below the bottommost surface of the lossy tissue-simulant phantom. Frequency = 5.25 GHz.

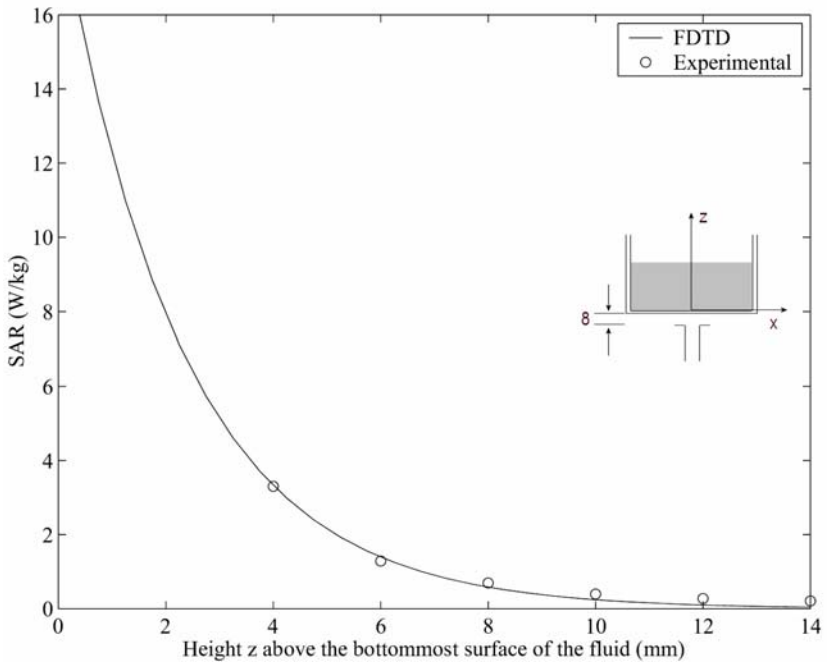

a. Variation of SAR along the z-axis.

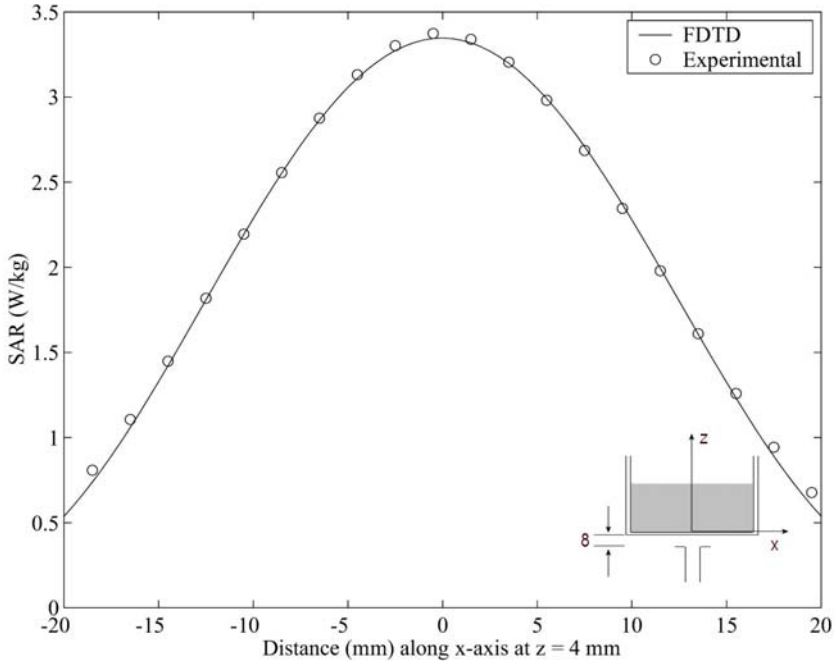

b. Variation of SAR along the x-axis parallel to the broader dimension of the waveguide at height z = 4 mm.

Fig. 4. Comparison of the measured and calculated SAR variations for a planar phantom of base thickness 2.0 mm and internal dimensions 30.5 × 41.9 × 20 cm for a WR 187 open-ended waveguide radiator placed 10 mm below the bottommost surface of the lossy tissue-simulant phantom. Frequency = 5.8 GHz.

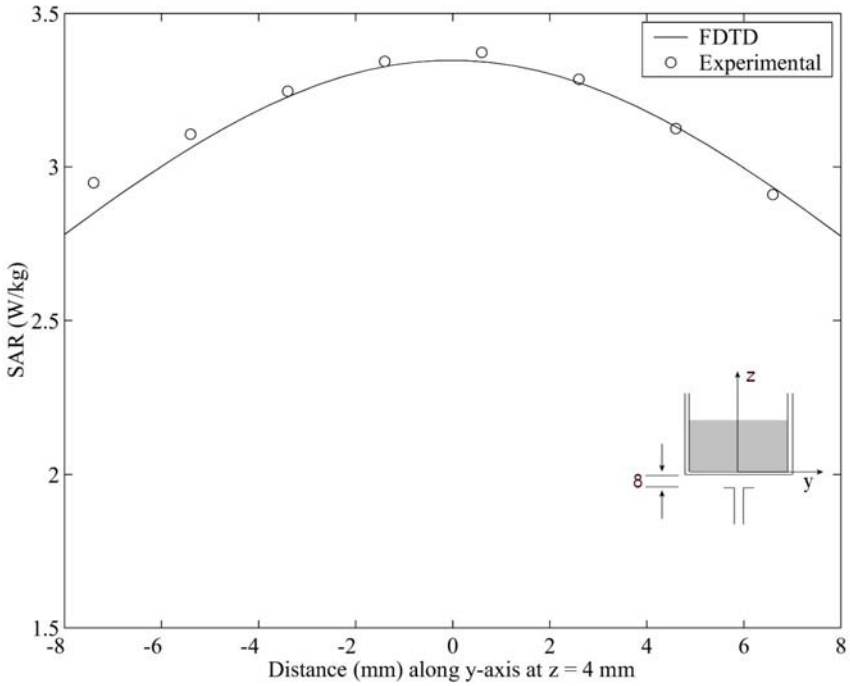

c. Variation of SAR along the y-axis parallel to the narrower dimension of the waveguide at height z = 4 mm.

Fig. 4. Comparison of the measured and calculated SAR variations for a planar phantom of base thickness 2.0 mm and internal dimensions 30.5 × 41.9 × 20 cm for a WR 187 open-ended waveguide radiator placed 10 mm below the bottommost surface of the lossy tissue-simulant phantom. Frequency = 5.8 GHz.

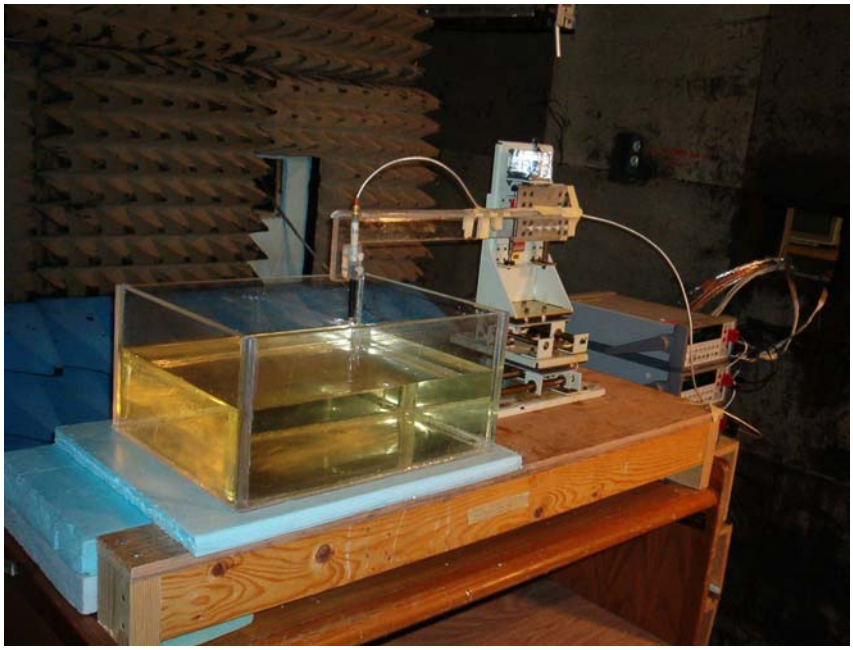

Fig. 5. Photograph of the planar model with the 3-D stepper motor system used for measurement of SAR variation for comparison with FDTD calculations.

A triaxial Narda Model 8021 E-field probe is used to determine the internal electric fields. The positioning repeatability of the stepper motor system moving the E-field probe is within ± 0.1 mm. Outputs from the three channels of the E-field probe are dc voltages, the sum of which is proportional to the square of the internal electric fields ($|E_i|^2$) from which the SAR can be obtained from the equation: SAR = $\sigma(|E_i|^2)/\rho$, where σ and ρ are the conductivity and mass density of the tissue-simulant material, respectively [13]. The dc voltages for the three channels of the E-field probe are read by three HP 34401A multimeters and sent to the computer via an HPIB interface. The setup is carefully grounded and shielded to reduce the noise due to the electromagnetic interference (EMI).

B. ***E-Field Probe***

The nonperturbing implantable E-field probe used in the setup was originally developed by Bassen et al. [14] and is manufactured by L3/Narda Microwave Corporation, Hauppauge, NY as Model 8021 E-field probe. In the probe, three orthogonal miniature dipoles each of length approximately 2.5 mm are placed on a triangular-beam substrate. Each dipole is loaded with a small Schottky diode and connected to the external circuitry by high resistance ($2\ \mathrm{M}\Omega \pm 40\%$) leads to reduce secondary pickups. The entire structure is then encapsulated with a low dielectric constant insulating material. The probe thus constructed has a very small diameter (4 mm), which results in a relatively small perturbation of the internal electric field. The probe is rated for frequencies up to 3 GHz for tissue-simulant media, but is presently used for system validation at frequencies in the 5 to 6 GHz range. Consequently, the probe had to be checked for square-law performance, and isotropy for use at these higher frequencies.

1. **Test for Square-Law Region:** It is necessary to operate the E-field probe in the square-law region for each of the diodes so that the sum of the dc voltage outputs from the three dipoles is proportional to the square of the internal electric field ($|E_i|^2$). Fortunately, the personal wireless devices such as the PCs induce SARs that are generally less than 5-6 W/kg even for closest locations to the body. For SAR measurements, it is, therefore, necessary that the E-field probe be checked for square-law behavior for SARs up to such values that are likely to be encountered. Such a test may be conducted using a canonical lossy body such as a rectangular box used here. By varying the radiated power of the waveguide, the output of the probe should increase linearly with the applied power for each of the test locations.

   Shown in Fig. 6a and b are the results of the tests performed to check the square-law behavior of the E-field probe used in our setup at 5.25 and 5.8 GHz, respectively. Used as the radiator is the WR 187 waveguide placed at a distance of 8 mm below the base of the planar phantom (10 mm below the bottom surface of the tissue-simulant fluid as recommended in [6]).

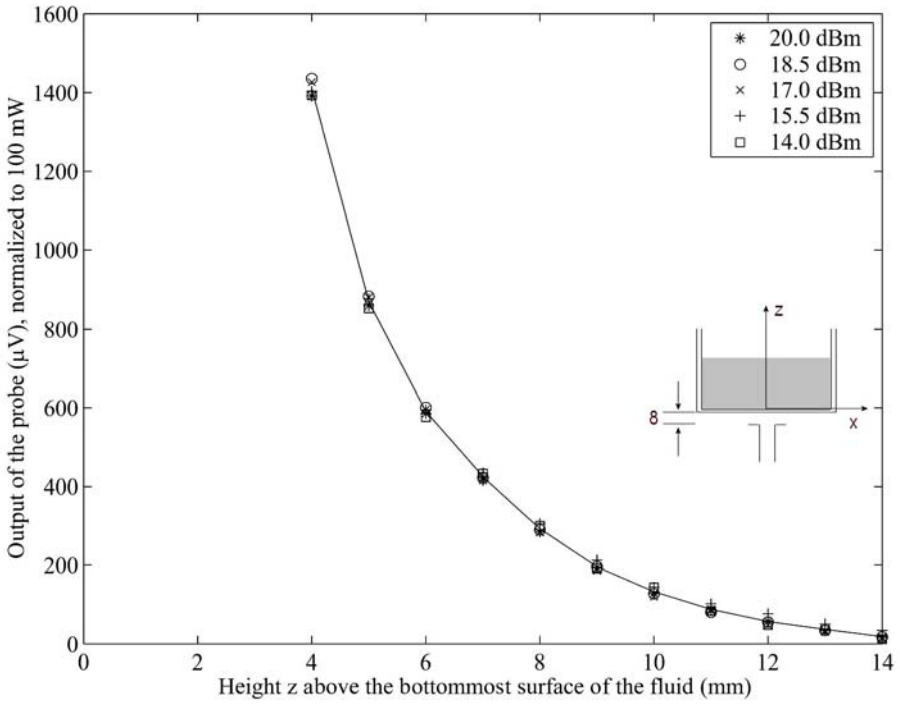

a. Test for square-law behavior at 5.25 GHz.

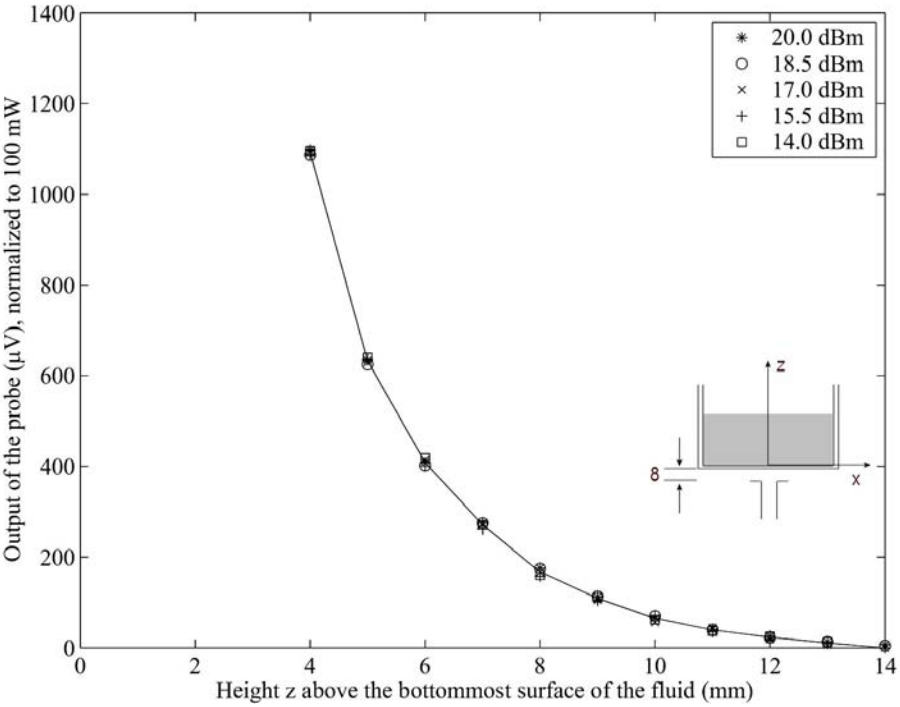

b. Test for square-law behavior at 5.8 GHz.

Fig. 6. Variation of the output voltage (proportional to $|E_i|^2$) for different radiated powers normalized to 100 mW (20 dBm).

Since the dc voltage outputs of the probe are fairly similar when normalized to a radiated power of 100 mW, the square-law behavior is demonstrated and an output voltage that is proportional to $|E_i|^2$ is obtained within ± 2.2% both at 5.25 and 5.8 GHz.

2. **Test for Isotropy of the Probe:** Another important characteristic of the probe that affects the measurement accuracy is its isotropy. Since the orientation of the induced electric field is generally unknown, the E-field probe should be relatively isotropic in its response to the orientation of the E-field. Shown in Fig. 7a and b are the test results of the E-field probe used in our setup at 5.25 and 5.8 GHz, respectively. The E-field probe was rotated around its axis from 0-180° in incremental steps of 15°. Because of the alternating nature of the fields, angles of θ and 180° + θ are identical, hence 0-165° rotation of the E-field probe was considered to be adequate to cover the entire 360° rotation of the probe. As seen in Fig. 7a and b, an isotropy of less than ± 0.18 dB (± 4.3%) was observed for this E-field probe both at 5.25 and 5.8 GHz.

3. **Calibration of the E-Field Probe:** Since the voltage output of the E-field probe is proportional to the square of the internal electric field ($|E_i|^2$), the SAR is, therefore, proportional to the voltage output of the E-field probe by a proportionality constant C. The constant C is defined as the calibration factor and is frequency and material dependent. It is measured to calibrate the probe at the various frequencies of interest using the appropriate tissue-simulating materials for the respective frequencies.

   Canonical geometries such as waveguides, rectangular slabs, and layered or homogeneous spheres have, in the past, been used for the calibration of the implantable E-field probe [15-17] albeit at lower frequencies. Since the FDTD method has been carefully validated to solve electromagnetic problems for a variety of near-field exposure geometries [18], we were able to calibrate the Narda E-field probe by comparing the measured variations of the probe voltage (proportional to $|E_i|^2$) against the FDTD-calculated variations of the SARs for the planar phantom of base thickness 2.0 mm ($\varepsilon_r = 2.56$) and internal dimensions 30.5 × 41.9 × 20 cm irradiated by the WR 187 waveguide placed below this phantom as previously described in Section. II. Shown in Figs. 6a, b and 7a, b are the comparisons between the experimentally measured and FDTD-calculated variations of the SAR distributions in the tissue-simulant fluid. Since there are excellent agreements between the calculated SARs and the measured variations of the voltage outputs of the E-field probe, it is possible to calculate the calibration factors at the respective frequencies by fitting the measured data to the FDTD-calculated results by means of the least mean-square error (LMSE) method. For the Narda Model 8021 E-field probe used in our setup, the calibration factor is determined to be 2.98 (mW/kg)/μV ± 5% both at 5.25 and 5.8 GHz, respectively.

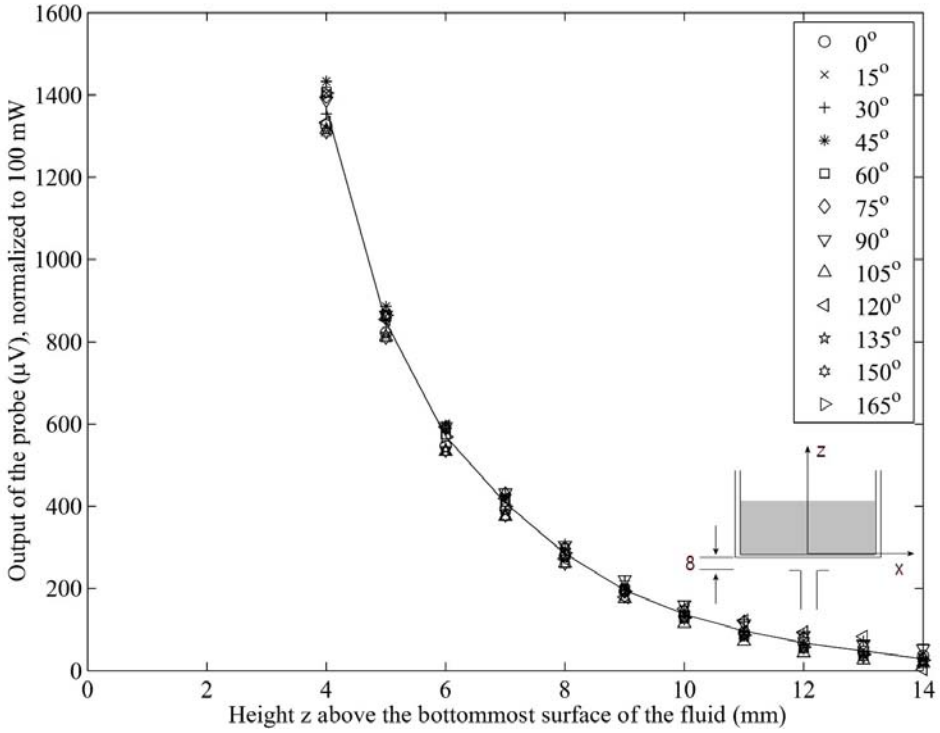

a. 5.25 GHz.

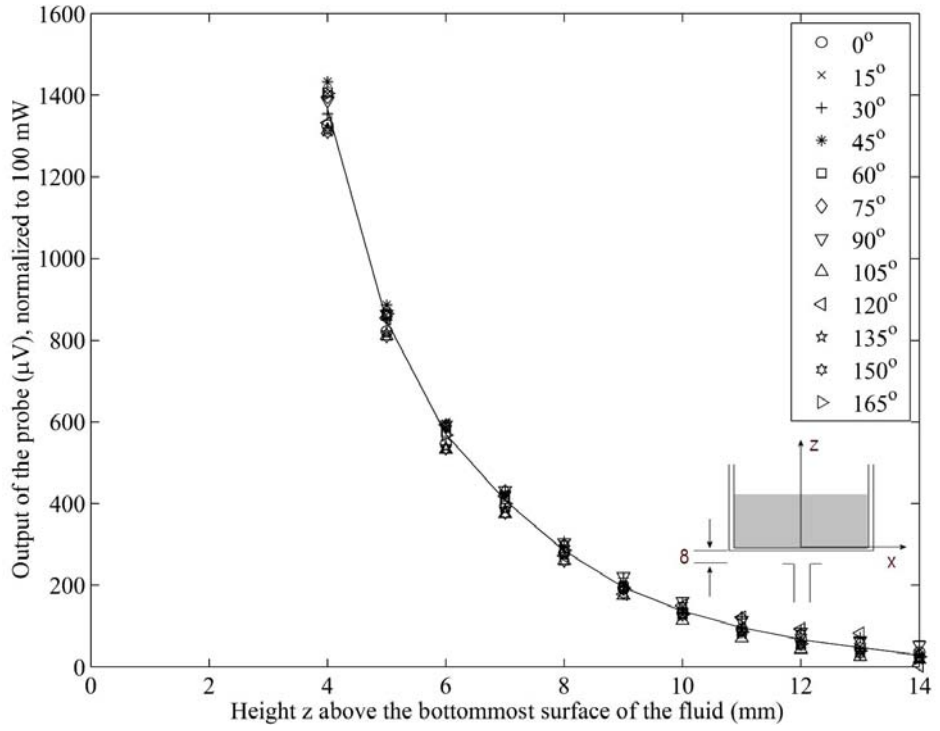

b. 5.8 GHz.

Fig. 7. Test for isotropy.

V. Need for Extrapolation

Because of the physical separation of the three orthogonal pickup dipoles from the tip of the E-field probe, the SAR measurements cannot be taken any closer than about 3 mm from the bottom surface of the phantom fluid. As given in Figs. 8 and 9, we have measured the SARs with 2 mm resolution at heights of 4, 6, 8, 10, 12 and 14 mm above the bottom surface of the phantom fluid. We have tried second-, third-, fourth-, and fifth-order polynomial least-square fits to extrapolate the measured data to obtain SARs closer to the bottom of the lossy fluid. As seen in Figs. 8 and 9, the second- and third-order polynomials underestimate the SARs while the fifth-order polynomial overestimates the SAR distribution. An excellent least-square fit to the numerically-calculated SAR variations is obtained by using a fourth-order polynomial to extrapolate the measured data both at 5.25 and 5.8 GHz.

After identifying the region of the highest SAR, the SAR distributions were measured with a finer resolution of 2 mm in order to obtain the peak 1 cm^3 or 1-g SAR. Here too, the SAR measurements were performed for the xy planes at heights z of 4, 6, 8, 10, 12, and 14 mm from the bottom surface of the body-simulant fluid. The SARs thus measured were extrapolated using a fourth-order least-square fit to the measured data to obtain values at 1, 3, 5, 7, and 9 mm height and used to obtain peak 1-g SARs. For a radiated power of 100 mW, the SARs thus obtained with 2 mm resolution for xy planes at heights z of 1, 3, 5, 7, and 9 mm for the peak SAR region of volume 10 ×10 × 10 mm were used to obtain peak 1-g SAR at 5.25 and 5.8 GHz, respectively. The experimentally-determined peak 1-g SARs for 100 mW of radiated power of 3.678 and 3.947 W/kg are extremely close to the FDTD-calculated 1-g SARs for this waveguide irradiator of 3.580 and 3.946 W/kg at 5.25 and 5.80 GHz, respectively.

V. Conclusions

We have developed an open-ended waveguide irradiation system for validation of the SAR measurement system and/or for E-field probe calibration in the 802.11a frequency band 5.15 to 5.825 GHz. A fourth-order polynomial least-square fit to the experimental data gives SAR variations close to the bottom surface of the phantom that are in excellent agreement with those obtained using the FDTD method. The experimentally-determined peak 1-g SARs are within 1 to 2 percent of those obtained using the FDTD numerical calculations.

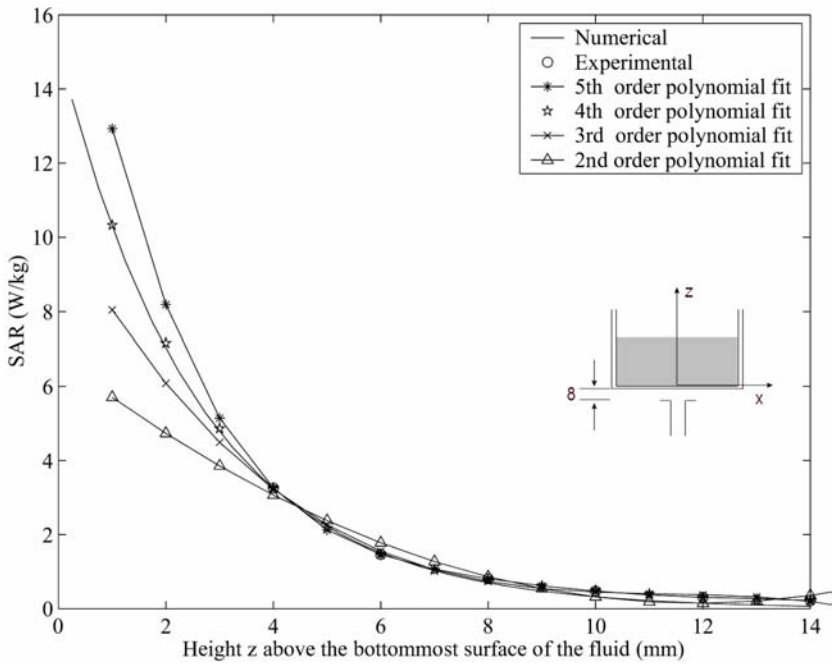

Fig. 8. Comparison of the experimentally measured and FDTD-calculated variation of the SAR with depth in the body-simulant planar phantom at 5.25 GHz. Also shown are the SARs extrapolated from experimental values to heights of 1, 3, 5, 7 and 9 mm above the bottom of the phantom using second-, third-, fourth-, and fifth-order least-square fit polynomials.

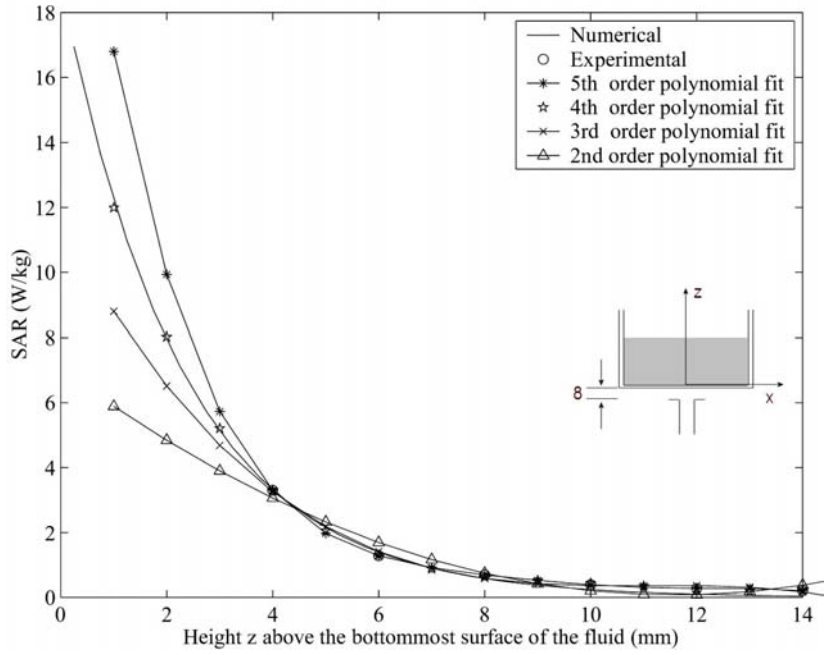

Fig. 9. Comparison of the experimentally measured and FDTD-calculated variation of the SAR with depth in the body-simulant planar phantom at 5.8 GHz. Also shown are the SARs extrapolated from experimental values to heights of 1, 3, 5, 7 and 9 mm above the bottom of the phantom using second-, third-, fourth-, and fifth-order least-square fit polynomials.

REFERENCES

1. IEEE Std. C95.1, "IEEE Standard for Safety Levels with Respect to Human Exposure to Radiofrequency Electromagnetic Fields, 3 kHz to 300 GHz," Institute of Electrical and Electronics Engineers, Piscataway, NJ, 1999.

2. ICNIRP (International Commission on Non-Ionizing Radiation Protection), "Guidelines for limiting exposure to time-varying electric, magnetic, and electromagnetic fields (up to 300 GHz)", *Health Physics*, Vol. 74, pp. 494-522, 1998.

3. IEEE Standards Coordinating Committee 34 Draft Standard, "Recommended Practice for Determining the Peak Spatial-Average Specific Absorption Rate (SAR) in the Human Body Due to Wireless Communications Devices: Experimental Techniques," Institute of Electrical and Electronics Engineers, 2002.

4. CENELEC EN50361, "Basic Standard for Measurement of Specific Absorption Rate Related to Human Exposure to Electromagnetic Fields from Mobile Telephones (300-MHz-3 GHz), CENELEC European Committee for Electrotechnical Standardization, rue de Stassart 35, B-1050, Brussels, Belgium.

5. IEC TC 106/PT62209, "Evaluation of Human Exposure to Radiofrequency Fields from Handheld and Body-Mounted Wireless Communications Devices in the Frequency Range of 30 MHz to 6 GHz: Human Models, Instrumentation Procedures," Draft Standard in preparation, 2003.

6. U.S. Federal Communications Commission (FCC), "Additional Information for Evaluating Compliance of Mobile and Portable Devices with FCC Limits for Human Exposure to Radiofrequency Emissions," Supplement C Edition 01-01 to OET Bulletin 65 Edition 97-01, June 2001.

7. A. Taflove (Ed.), *Advances in Computational Electrodynamics: The Finite-Difference Time-Domain Method,* Artech House, Boston, MA, 1998.

8. A. Taflove and S. C. Hagness, *Computational Electrodynamics: The Finite-Difference Time-Domain Method*, Artech House, Boston, MA, 2000.

9. P. J. Dimbylow and S. M. Mann, "SAR Calculations in an Anatomically-Based Realistic Model of the Head for Mobile Communication Transceivers at 900 MHz and 1.8 GHz," *Physics in Med. and Biol.,* Vol. 39**,** pp. 1537-1553, 1994.

10. O. P. Gandhi and J. Y. Chen, "Electromagnetic Absorption in the Human Head from Experimental 6 GHz Handheld Transceivers," *IEEE Trans. on Electromag. Compat.,* Vol. 37, pp. 547-558, 1995.

11. M. A. Jensen and Y. Rahmat-Samii, "EM Interaction in Handset Antennas and a Human in Personal Communications," *Proc. IEEE,* Vol. 83, pp. 7-17, 1995.

12. M. Okoniewski and M. A. Stuchly, "A Study of Handset Antenna and Human Body Interaction, *IEEE Trans. on Microwave Theory and Tech,* Vol.. 44, pp. 1855-1864, 1996.

13. M. A. Stuchly and S. S. Stuchly, "Experimental Radio and Microwave Dosimetry, " in *Handbook of Biological Effects of Electromagnetic Fields,*, 2nd ed., C. Polk and E. Postow, Eds. Boca Raton, FL: CRC, pp. 295-336, 1996.

14. H. I. Bassen and G. S. Smith, "Electric Field Probes -- a Review," *IEEE Trans. Antennas Propagat.,* Vol. AP-31, pp. 710-718, September 1983.

15. D. Hill, "Waveguide Techniques for the Calibration of Miniature Electric Field Probes for Use in Microwave Bioeffects Studies," *IEEE Trans. Microwave Theory Tech.,* Vol. MTT-30, pp. 92-94, 1982.

16. N. Kuster and Q. Balzano, "Energy Absorption Mechanism by Biological Bodies in the Near Field of Dipole Antennas Above 300 MHz," *IEEE Trans. Veh. Technol.,* Vol. 41, pp. 17-23, February 1992.

17. M. A. Stuchly, S. S. Stuchly, and A. Kraszewski, "Implantable Electric Field Probes – Some Performance Characteristics," *IEEE Trans. Biomed. Eng.,* Vol. BME-31, pp. 526-531, July 1984.

18. C. M. Furse, Q. S. Yu, and O. P. Gandhi, "Validation of the Finite-Difference Time-Domain Method for Near-Field Bioelectromagnetic Simulations," *Microwave and Optical Technology Letters*, Vol. 16, pp. 341-345, 1997.

APPENDIX D

Uncertainty Analysis

The uncertainty analysis of the University of Utah SAR Measurement System is given in Table D.1. Several of the numbers on tolerances are obtained by following procedures similar to those detailed in [3], while others have been obtained using methods suggested in [5].

Table D-1. Uncertainty analysis of the University of Utah SAR Measurement System.

Uncertainty Component	Uncertainty Value ± %	Probability Distribution	Divisor	C_i 1-g	Standard Unc. u_i ± %	ν_i
Measurement System						
Probe calibration	2.0	N	1	1	2.0	∞
Axial isotropy of the probe	4.0	R	√3	$(1\text{-cp})^{1/2}$	1.6	∞
Hemispherical isotropy of the probe	5.5	R	√3	$\sqrt{c_p}$	0.0	∞
Boundary effect	0.8	R	√3	1	0.5	∞
Probe linearity	3.0	R	√3	1	1.7	∞
System detection limits	1.0	R	√3	1	0.6	∞
Readout electronics	1.0	N	1	1	1.0	∞
Response time	0.0	R	√3	1	0.0	∞
Integration time	0.5	R	√3	1	0.3	∞
RF ambient conditions	0	R	√3	1	0	∞
Probe positioner mechanical tolerance	0.5	R	√3	1	0.3	∞
Probe positioning with respect to phantom shell	2.0	R	√3	1	1.2	∞
Extrapolation, interpolation, & integration algorithms for maximum SAR evaluation	5.0	R	√3	1	2.9	∞
Test Sample Related						
Device positioning	3	R	√3	1	1.7	11
Device holder uncertainty	3	R	√3	1	1.7	7
Output power variation – SAR drift measurement	5	R	√3	1	2.9	∞
Phantom and Tissue Parameters						
Phantom uncertainty – base thickness tolerance	10.0	R	√3	1	5.8	∞
Liquid conductivity – deviation from target values	0.4	R	√3	0.7	0.2	∞
Liquid conductivity – measurement uncertainty	1.5	R	√3	0.7	0.6	∞
Liquid permittivity – deviation from target values	0.8	R	√3	0.6	0.3	∞
Liquid permittivity – measurement uncertainty	3.5	R	√3	0.6	1.2	∞
Combined Standard Uncertainty		RSS			8.3	
Expanded Uncertainty (95% Confidence Level)					± 16.6	